Imaging Earth's Seismic Response at Long Periods

PAGES 449, 451, 452

Peter M. Shearer

At long periods, seismic waves generated by different earthquakes can be used to construct a single global image of Earth's response to seismic energy. This image (Figure 1) plots the expected ground motion at a point on Earth's surface as a function of time and distance to the earthquake. The various streaks on the plot represent different types of seismic waves, each of which travels at a different speed and arrives at a different time.

Stacking—a process that averages and combines seismograms from a number of different source-receiver locations—was used to create the image from thousands of individual records. The result is a direct view of the average wave field that can be used both as a teaching tool for illustrating the properties of the wave field and as a guide to further study.

Global Stacking

The Earth's deep interior is nearly spherically symmetric. Beneath the upper few tens of kilometers where surface features lie, the variations in properties, such as density and seismic velocity, at a particular radius are fairly small. Given this simplicity, seismologists in the early part of the century were able to obtain good estimates of Earth's average radial velocity structure—even from sparse data sets—by measuring the arrival times of seismic waves as a function of distance between source and receiver.

More recently, seismologists have used the growing number of global seismic stations to resolve Earth's more subtle three-dimensional structure. Nevertheless, Earth's average one-dimensional response to seismic energy remains of interest since it defines the dominant features observed on seismograms and is generally used as a start-

ing point for studies of three-dimensional perturbations.

Stacking is one way to resolve Earth's one-dimensional seismic response at a given source-receiver distance. It works best at relatively low frequencies, since they are least sensitive to three-dimensional perturbations. At higher frequencies, the effect of aspherical structure is more pronounced, causing time shifts and waveform distortion that prevent the coherent stacking of waveforms. At

periods of about 25 s, the Earth's major body wave arrivals can be imaged [*Shearer*, 1991a], and some stacks reveal weak, secondary arrivals resulting from reflections off discontinuities in the upper mantle [*Shearer*, 1991b].

Surface waves are harder to image than body waves in global stacks since lateral velocity variations often cause time shifts in surface-wave arrivals of tens of seconds, compared to the much smaller shifts observed for most body-wave phases. However, at periods of 60 s and longer, it is possible to produce a coherent image of both body- and surface-wave arrivals extending for many hours after the earthquake origin times.

The IDA Data Set

The International Deployment of Accelerometers (IDA) Network [*Agnew*, 1986] is a global array of about 20 digital vertical-com-
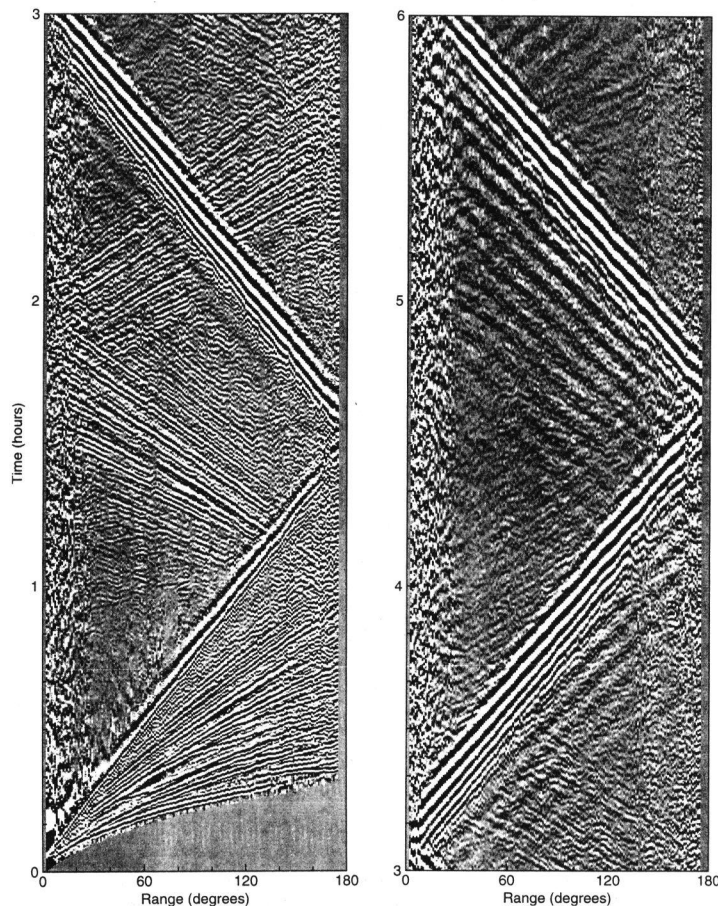

Fig. 1. An image of Earth's long-period seismic response on vertical component seismographs as a function of time and distance to an earthquake. Positive amplitudes are shown as black, and negative amplitudes are shown as white. Since different types of seismic waves (for example, compressional, shear, and surface waves) travel at varying speeds, they arrive at different times for a receiver at a particular range. Numerous body- and surface-wave arrivals are clearly visible as streaks in this image. Figure 3 identifies the main features in this plot.
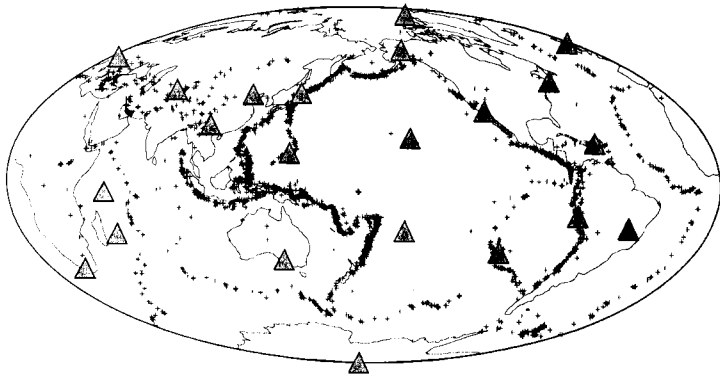
Institute of Geophysics and Planetary Physics, Scripps Institution of Oceanography, San Diego, La Jolla, CA 92093-0225

Fig. 2. Locations of the IDA stations and the 2906 events used in the global stack.
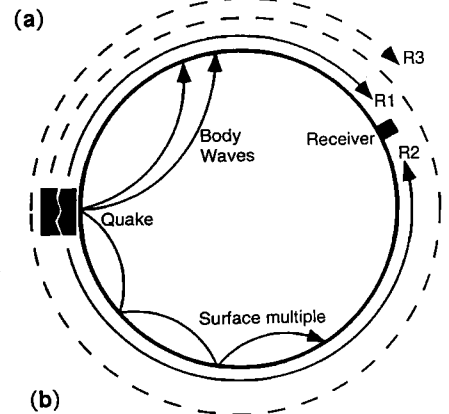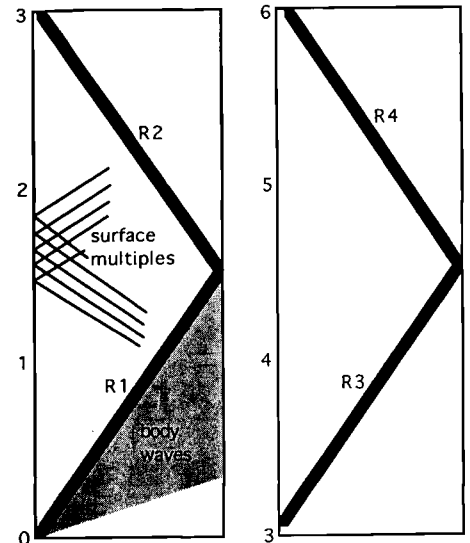

(a)

(b)

Fig. 3. a) A key to the main features of the image shown in Figure 1. b) The path geometry for the Rayleigh surface-wave arrivals R1, R2, and R3 at a source-receiver range of about 150°. The first Rayleigh wave arrival R1 travels along the minor great circle arc, whereas the second arrival, R2, travels along the major arc.

ponent accelerometers that record at very long periods (T≥60 s). Its primary purpose is to record Earth's normal modes, but it also provides data on direct surface- and body-wave arrivals.

Figure 2 shows the distribution of IDA stations, not all of which were operational at the same time. The number of operating stations increased gradually during the early 1980s with an average of about 15 stations recording events during 1985. Although station distribution is sparse, global coverage is good. The IDA data in Figure 1 are from 1981 to 1991; surface ground motion was recorded every 10 s.

The most suitable earthquakes for stacking are isolated in time from other events and are shallow, since complications due to surface reflections are avoided. Of the 7731 earthquakes in the Harvard centroid-moment tensor catalog [e.g., *Dziewonski and Woodhouse*, 1983] recorded between 1981 and 1991, 2906 events are selected that are both less than 100 km deep and well separated in time from comparably sized events. The locations of these sources are shown in Figure 2.

Seismograms for each event are extracted and high-pass filtered to periods less than 500 s to remove Earth tides. The amplitudes of the P and PP arrivals on these seismograms are measured and compared to the noise level preceding the arrival (P is the direct compressional wave arrival, PP is the first surface multiple of P). Only those seismograms in which this local signal-to-noise ratio exceeds a threshold value are saved for subsequent processing. This avoids contaminating the stack with noisy seismograms that lack clear seismic signals.

Stacking Procedure

The waveforms in the IDA records vary as a function of earthquake depth and focal mechanism. However, a large fraction of the traces are very similar and can be stacked coherently if the polarity and timing of the seismogram is adjusted.

The stacking strategy used to construct Figure 1 is iterative. First, a target seismogram is assumed at 80°. Each seismogram at ranges between 80° and 81° is cross-correlated with the target trace to determine the maximum correlation coefficient r and corresponding time shift and scaling. Polarity reversals are permitted in finding the maxi-

mum r. The seismograms are stacked using the appropriate time shifts and weighting each seismogram by r, and then the trace resulting from this stack is used as a new target and the process is repeated until a stable result is obtained. The result for the 80°-81° interval is used as the initial target seismogram for the adjacent range intervals, and the stacking procedure continues to different ranges until the complete image is formed.

This weighting scheme emphasizes the seismograms that agree in shape with the final stacked image. To produce the most coherent result, some additional refinements are made. One problem is that the time and polarity shifts that are optimal for P may not be best for other arrivals. For example, S and surface-wave polarities are not, in general, predictable from a single P polarity observation.

Somewhat surprisingly, however, rough images of these later phases can be obtained in stacks from seismograms adjusted using P phases alone. The coherence in the final stack is improved by repeating the alignment process described above separately within a sequence of 10-min windows. The complete image is then produced by smoothly patching together these locally optimized stacks.

Seismogram amplitudes vary considerably as a function of both range and time into the seismogram. To show results from 0°-180° on a single plot, each seismogram is scaled to have the same root-mean-square amplitude within the first 100 min. To compensate for amplitude decay with time in the final image, amplitude is scaled by $t^{1/2}$ where t is in hours from the earthquake origin time.

The image is noisiest at ranges below 30° and beyond 150°. There are much less data available at these ranges due to the spherical geometry; the gap beyond 175° results from a lack of observations at both sides of the Earth. In addition, the results at close ranges are contaminated by instrument clipping, in which large amplitudes are truncated to smaller values, and nonlinear time-dependent responses to large amplitudes.

Interpretation

Figure 3a labels the main features in the stacked image. Most prominent is the Rayleigh wave, which travels along Earth's surface. This wave appears in the image many times as it propagates around the globe. R1 is the first seg-

ment of the Rayleigh wave. When the wave travels past 180°, it begins traveling back toward the source and is called R2. Once it passes 360°, it is again traveling away from the source and is designated R3.

Figure 3b shows these path geometries for a receiver located about 150° away from an earthquake. Body-wave arrivals are also visible in the stacked image. The major body-wave phases can be seen in the triangular-shaped region before R1. These phases may be identified by consulting standard travel-time tables or the plots given by *Shearer* [1991a] and *Earle and Shearer* [1994].

Additional body-wave arrivals can be seen between R1 and R2. These include some P phases, but most prominent are the high-order S surface multiples and the families of S-to-P converted phases that they spawn upon each surface reflection. These can be traced to beyond 720° and are the major source of seismic energy between the Rayleigh wave arrivals. In the surface wave literature, these arrivals are termed overtone
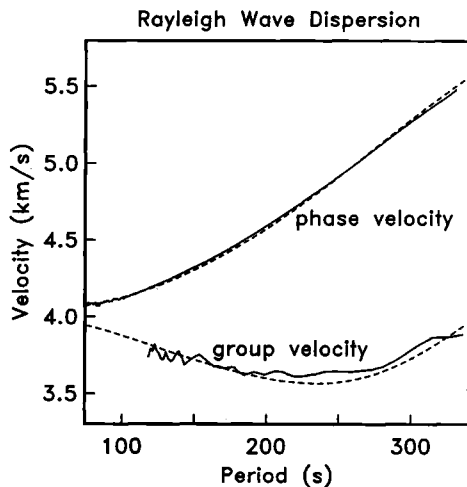
Rayleigh Wave Dispersion

Fig. 4. Rayleigh wave phase and group veloc-
ity versus period, as measured from R2 in the
stacked image (solid lines), and as predicted
by model 1066A (dashed lines). Note that the
phase velocity is higher than the group veloc-
ity and that a minima in group velocity exists
for waves at periods of about 240 s.

packets and are sometimes referred to as X
phases [e.g., Tanimoto, 1987].

The dispersion in the surface waves is
clearly apparent, particularly in the latter
part of the image. Very long period (≥300 s)
waves travel the fastest, arriving before the
pronounced shorter-period banding in the
Airy phase. The high amplitude of the Airy
phase results from a local minima in the group
velocity versus frequency curve near 240 s.

The difference between phase and group
velocity can be seen clearly in the image of
the Airy phase. The lines of constant phase,
defined by the peaks and troughs in the seis-
mograms, are not parallel to the overall
direction of energy transport. Rather they cut
across at a more horizontal orientation, since
the phase velocity is higher than the group ve-
locity.

These relationships are illustrated in Fig-
ure 4, which plots phase and group velocity
as a function of period from 75 to 340 s, as
measured from the R2 arrival in the stacked
image. The phase velocity is determined by
computing the Fourier spectrum as a func-
tion of range for a suitable window around
R2 and fitting the change in phase versus
range for each frequency component. The
group velocity curve is obtained by differenti-
ating the phase velocity curve using the
appropriate conversion to wavenumber k.

For comparison, predicted results for
model 1066A [Gilbert and Dziewonski, 1975]
are shown as dashed lines. The slight dis-
agreement with the 1066A curves is not
significant since lateral variations of several
percent are observed in Rayleigh wave ve-
locities and the stacking procedure does not
attempt to produce an unbiased global aver-
age.

The image shown in Figure 1 is available
as a poster from Geological Data Center,
Scripps Institution of Oceanography 0223,
University of California at San Diego, La Jolla,
CA 92093-0223. The Postscript file may be ob-
tained directly from the author (Internet:
pshearer@ucsd.edu).

References

Agnew, D. C., J. Berger, W. E. Farrell,
J. F. Gilbert, G. Masters, and D.
Miller, Project IDA: A decade in review,
Eos Trans. AGU, 67, 203, 1986.
Dziewonski, A. M., and J. H. Wood-
house, An experiment in systematic study
of global seismicity: Centroid-moment ten-
sor solutions for 201 moderate and large
earthquakes of 1981, J. Geophys. Res.,
88, 3247, 1983.
Earle, P. S., and P. M. Shearer, Charac-
terization of global seismograms using an
automatic-picking algorithm, Bull. Seismol.
Soc. Am., 84, 366, 1994.
Gilbert, F., and A. M. Dziewonski, An applica-
tion of normal mode theory to the retrieval
of structural parameters and source mecha-
nisms from seismic spectra, Philos. Trans. R.
Soc. London, Ser. A, 278, 187, 1975.
Shearer, P. M., Imaging global body wave
phases by stacking long-period seismograms,
J. Geophys. Res., 96, 20,353, 1991a.
Shearer, P. M., Constraints on upper mantle
discontinuities from observations of long-pe-
riod reflected and converted phases, J. Geo-
phys. Res., 96, 18,147, 1991b.
Tanimoto, T., The three-dimensional shear wave
structure in the mantle by overtone waveform
inversion, I. Radial seismogram inversion, Geo-
phys. J. R. Astron. Soc., 89, 713, 1987.

Solar Influences on Global Change Get Their Day in the Sun

PAGES 449, 451

Many doomsayers—including some of
the world's best and brightest astrophysi-
cists—maintain that the Sun will someday
burn up the Earth and bring an end to life as
we know it. Even if this prophecy were to
come true, the Earth wouldn't become unin-
habitable for more than a billion years,
according to current estimates. A much more
immediate problem that we could face is the
effects the Sun may have on global climate
change.

A recent report by the National Research
Council (NRC) delved into this very issue, as
a result of its being identified as one of seven
primary science elements by the U.S. Global
Change Research Program. Some of the re-
port's authors hope that the findings (box)
may help develop a strategy for coordinating
climate change research in the United States.

Until recent years, the natural compo-
nents of global change—those that are not
human-induced—had been relatively over-
looked in the overall study of climate

change, some researchers maintain. For a
start, studies of solar changes had been lim-
ited by scientists' inability to directly
measure the Sun's radiation from space. Di-
rect measurements are impossible from
ground-based observatories and awaited
technological developments. During the 80s,
measurements from spacecraft confirmed an
11-year cycle of the Sun and demonstrated
that the so-called solar "constant" really is
not a constant after all.

"Now we have observations that show be-
yond a doubt that solar activity varies in
terms of both total radiation and spectral ra-
diation," says Judith Lean, a physicist at the
Naval Research Laboratory.

Yet today, the question remains "does it
[solar radiation] vary by larger amounts and
on longer timescales?" says Lean who
chaired the NRC group that issued the report
entitled "Solar Influences on Global Change."

Circumstantial evidence, from both cli-
mate and solar data, suggests that the Sun's

Scientific Conclusions on Solar
Influences on Global Change
Issued by National Research Council Panel

• Solar variations directly force global
surface temperature.
• Solar variations modify ozone and the
middle atmosphere structure.
• Solar variability effects in Earth's upper
atmosphere may possibly couple to the
middle atmosphere and the biosphere.
• It is unknown whether solar variability
effects in the Earth's near-space environ-
ment couple to the biosphere.
• The knowledge of the variable Sun
needs to be improved to understand
and predict solar influences on global
change.

activity is likely changing on longer times-
cales. However, scientists don't know by how
much or what the implications of solar vari-
ations may be.

Most global change researchers believe
that greenhouse gases provide a warming ef-
fect, and that various aerosols provide a
cooling effect; but the Sun could do either,
Lean says.

Indeed, the other question the NRC report
addresses is whether the Sun's variations